



This is the accepted manuscript made available via CHORUS. The article has been published as:

Strain-dependent spin Hall magnetoresistance in the multiferroic antiferromagnet math xmlns="http://www.w3.org/1998/Math/MathML">msub>mi >BiFeO/mi>mn>3/mn>/msub>/math>

D. Sando, S. Chen, O. Paull, B. Xu, J. J. L. van Rijn, C. Xu, S. Xu, F. Appert, J. Juraszek, L. Bellaiche, V. Nagarajan, and T. Banerjee

Phys. Rev. Materials 8, L071401 — Published 12 July 2024

DOI: 10.1103/PhysRevMaterials.8.L071401

Strain-dependent spin Hall magnetoresistance in the multiferroic antiferromagnet BiFeO₃

D. Sando^{1,2,3,*,+}, S. Chen^{4,+}, O. Paull^{2,3}, B. Xu⁵, J. J. L. van Rijn⁴, C. Xu⁶, S. Xu⁵, F. Appert⁷, J. Juraszek⁷, L. Bellaiche^{3,5}, V. Nagarajan^{2,3}, T. Banerjee^{3,4,*}

¹The MacDiarmid Institute for Advanced Materials and Nanotechnology, School of Physical and Chemical Sciences, University of Canterbury, Christchurch 8041 New Zealand ²School of Materials Science and Engineering, UNSW Sydney, Kensington 2052, Australia ³Australian Research Council Centre of Excellence in Future Low Energy Electronics, Australia ⁴University of Groningen, Zernike Institute for Advanced Materials, 9747 AG Groningen, The Netherlands

⁵Jiangsu Key Laboratory of Thin Films, School of Physical Science and Technology, Soochow University, Suzhou 215006, China

⁶Department of Physics and Institute for Nanoscience and Engineering, University of Arkansas, Fayetteville, AR, USA

⁷Univ Rouen Normandie, INSA Rouen Normandie, CNRS, Normandie Univ, GPM UMR 6634, F-76000 Rouen, France

*These authors contributed equally

Email: daniel.sando@canterbury.ac.nz , t.banerjee@rug.nl

Abstract

The spin Hall magnetoresistance (SMR) of antiferromagnetic BiFeO₃ thin film surfaces is investigated. SMR consistent with weak ferromagnetic order in films fabricated on (001) SrTiO₃ (R' BFO) and LaAlO₃ (T' BFO) substrates is found, albeit with different temperature dependencies. For T' BFO, the SMR is enhanced at room temperature, and decays with reduced temperatures. By contrast, R' BFO shows a monotonic decrease in SMR response with increasing temperature, mirroring the trend of a weak ferromagnet. Density functional theory shows that this intriguing difference originates due to the different octahedral rotation patterns in R' and T' BFO and their coupling to the applied magnetic field and spin degrees of freedom.

Bismuth ferrite (BiFeO₃ - BFO), a widely studied multiferroic oxide, has been a fertile playground for understanding electric field manipulation of magnetism [1–3]. The sensitivity of BFO's crystal structure to epitaxial constraint is well established [4,5]: large in-plane compressive strain induces a rhombohedral-like (R') to tetragonal-like (T') phase transition [6], with concomitant modification of ferroelectric, magnetic, and electromechanical properties [7]. Spin-lattice coupling effects in BFO have been widely studied [8–11].

More recently, BFO, an antiferromagnet (AFM) with a net weak ferromagnetism (FM) [12], has also garnered attention for its magnonic response [13,14]. Electrical generation and propagation of magnons forms a major thrust in developing antiferromagnet-based spintronics [15]. Parsonnet *et al.* recently studied magnons in epitaxial BFO thin films [16]. Using the spin Seebeck effect, they showed that magnon propagation was hindered by repeated scattering at ferroelectric/magnetic domain walls, revealing that domain morphology (of both magnetic and ferroelectric order parameters) and magnetic anisotropy govern magnon propagation. Epitaxial strain is known to induce prominent changes to the crystal structure in BFO (showcased in Fig. 1). The close link of the ferroelectric polarization and magnetic order to the crystallographic structure is thus expected to yield differences in magnonic response of T' BFO as compared to R' BFO. Moreover, the role of magnetic anisotropy on the magnetoresistance (MR) in BFO has important implications in magnetoelectrically coupled magnonic devices based on BFO [17].

In this Letter, we demonstrate strain-induced phase tuning of the spin Hall magnetoresistance (SMR) in epitaxial BFO layers. We show that the surface magnetic order is dramatically different for T' vs. R' ferroelectric structural phase as electrically read out using SMR. Whilst surprisingly the SMR suggests a ferromagnetic surface state for both R' and T' BFO, the temperature dependencies show stark differences. In T' BFO, the SMR signal is enhanced at room temperature, and it decays with reduced temperatures. By contrast, in R' BFO the SMR response decreases upon increasing temperature, essentially mirroring the temperature trend of the weak FM. We understand these differences in the framework of the weak magnetic moments but with markedly distinct origin in the two BFO phases by incorporating the DFT findings - in T' BFO the moment induced directly by the field gives the SMR response, while in R' BFO, the weak magnetic moment mediated by the antiferromagnetic (L) vector dominates the behavior. Our results demonstrate that (i) strain and/or phase engineering can be harnessed to modulate the SMR signal and its temperature dependence, ii) mesoscale BFO devices show promise for spintronic and magnonic technologies, and iii) one must account for weak FM in antiferromagnets in developing AFM spintronic devices.

SMR is an established method to read out the surface magnetic order in magnetic insulators (MIs) [18–21], making it a powerful interface-based technique to fingerprint magnetic anisotropy by electrical means. A charge current in a heavy metal (such as Pt) generates a transverse spin current through the spin Hall effect, yielding spin accumulation at the Pt surface [Fig. 1 (a)]. At the interface between the MI and Pt, the spins of the Pt electrons transfer their angular momentum, dependent on the magnetization orientation of the MI layer. Consequently, the spin current is absorbed (reflected) when the interfacial magnetic moments are oriented perpendicular (parallel) to the spin accumulation. The absorbed spin currents exert a spin transfer torque on the adjacent MI layer and dissipate, yielding a detectable increase in the Pt resistivity through the inverse spin Hall effect. An applied magnetic field H modifies the orientation of the magnetization in the MI layer, thereby modulating the resistance of the Pt layer. Figure 1(b) depicts the typical measurement geometry. In ferromagnets (FM) with small anisotropy, the magnetization vector **M** follows the rotating external H, resulting in an angular dependence of the resistance, defined as positive SMR [Fig. 1(c)] [22]. In contrast, in some AFM insulators, negative SMR has been observed [23,24]. Here, the Néel vector L remains orthogonal to the applied magnetic field, which, when compared to the positive SMR case, leads to a 90-degree phase shift in the angular dependence. The phase alignment in SMR can thus be exploited as a fingerprint to distinguish between FM and AFM interfaces.

Given that SMR probes surface magnetic states, it offers advantages over traditional volume averaged techniques such as neutron diffraction [25–28] Mössbauer spectroscopy [14,29,30], and Raman spectroscopy [13,14,31,32] when studying thin film-based devices. Such studies on multiferroic devices promise a new paradigm of electrically controlled spintronics, since 1) SMR can be applied to the understanding of magnon transport [24]; 2) SMR as a probe of surface magnetism makes it highly susceptible to distinguish strain-induced changes in spin order; 3) it is an all-electrical probe and thus an attractive approach for low-energy spintronic devices.

Our first insights come from density functional theory (DFT) calculations, used to determine the preferred structural phases, magnetic ground states, and weak ferromagnetism (wFM) of BFO at zero applied magnetic (H) field, at 0 K [Figs. 1(d-f)]. The calculated energy of G-type and C-type AFM ordering as a function of strain [Fig. 1(d)] shows that under moderate strain (from -4 % to +2 %), R' BFO, the AFM ground state is G-type. Moreover, the L vector is parallel to $[1\bar{1}0]$ (not shown) (pseudocubic indices are used throughout). In contrast, at high compressive strain (-4 % to -6 %, T' BFO), G-type and C-type AFM are essentially degenerate; however, for consistency with experiments on T' BFO [6], here we impose G-type AFM order.

The calculated components of the weak magnetization as a function of strain are shown in **Fig. 1(e)**. Under -1.5 % strain, corresponding to BFO grown on SrTiO₃ (STO), $M_x = M_y = +0.08 \, \mu_B$, while $M_z = -0.14 \, \mu_B$, yielding an **M** vector pointing approximately along [$11\overline{2}$] [**Fig. 1(g)**]. By contrast, under < -4.4% compressive strain (BFO on LaAlO₃ - LAO), $M_x = M_y = 0$, and the z component is very small (+0.04 μ_B), yielding **M** // [001] [**Fig. 1(h)**]. The direction of these **M** vectors is consistent with the rule that the wFM be proportional to the cross product between the AFM vector and the anti-phase oxygen octahedral tilting angle [33,34].

Since our DFT results find the magnetism for the T' and R' phases to be markedly different, it presents a unique opportunity to explore the potential of SMR in distinguishing these differences arising due to strain tuning (Fig. 2). We grew ~50 nm thick (001) BFO films by pulsed laser deposition onto STO and LAO substrates using conditions reported elsewhere [35–37]. We are uniquely able to fabricate phase pure T' BFO films up to 70 nm in thickness, with no trace of mixed phase striations [32]. This capability allows us to establish a clear contrast in behaviors of the T' and R' phases of BFO – and hence the remanent strain state – for a fixed film thickness of 50 nm, without complications from mixed R'/T' BFO. In the T' BFO, 50 nm is thin enough to be fully strained and avoid complications from dislocations and ferroelastic domain formations, but not so low as to suffer from interfacedriven size scaling effects. The uniform strain state moreover ensures a spatially homogeneous magnetic order that is picked up in a device geometry. Conversion electron Mössbauer spectroscopy [12] on comparable samples with 100% ⁵⁷Fe enrichment shows magnetic hyperfine sextets with an intensity ratio of peaks 2 and 3, R₂₃ close to 4, implying that the AFM vector is confined to the (001) plane [Fig. 1 (i,j)], consistent with L // $[1\bar{1}0]$ (Refs. [7,14,38]). The sextets for the two phases do not show asymmetry characteristic of a cycloidal modulation of the spins [14]. While the spectrum of R' BFO presents a hyperfine field close to that of bulk BFO (B_{hf} = 48.8 T), the T' BFO spectrum exhibits broader lines and a smaller hyperfine splitting with $\langle B_{hf} \rangle$ = 29.5 T, due to reduced magnetic interactions near the critical transition temperature of \sim 350 K [7].

We next performed temperature and field dependent SMR experiments. For this, Hall bars of 7 nm thick Pt were patterned by e-beam lithography onto T' and R' BFO samples. SMR manifests as a variation of the resistivity of the Pt electrode with the applied magnetic field and tracks the orientation of the surface magnetic moments with the spin accumulation at the interface between Pt and BFO. By probing the variation of the resistivity in the transverse (ρ_{xy}) and longitudinal (ρ_{xx}) directions under the rotation of the magnetic field **H** in the XY (rotation angle α), YZ (rotation angle

β), and XZ (rotation angle γ) planes (**Fig. 1b and S2** [39], see also references [40–42] therein), we measure a complete set of the angular dependence of the magnetoresistance (ADMR) for both the T' and R' BFO devices. We obtain a much cleaner response for the ρ_{xy} signal when compared to ρ_{xx} and thus focus on the ρ_{xy} and its dependence on temperature (The full set of measurements for ρ_{xx} are found in Figs. S3 and S4 [39]). **Figure 2(a)** shows the dependence of ρ_{xy} on the angle α [defined in **Fig. 1(b)**] at temperatures 50-370 K for T' BFO. The trend in ρ_{xy} is consistent with positive SMR, reminiscent of a FM response. Fitting the data to a model comprising two sinusoidal functions (**Figs. S1**, **S2** [39]) we extract the magnitude of the SMR $\Delta \rho_{xy}$ as a function of temperature [**Fig. 2(b)**]. SMR is not detected for T \leq 50 K, while for temperatures 200 K up to 370 K (the maximum for our setup), it monotonically increases.

By contrast, in the R' BFO sample, the 180° periodic α -dependent oscillations in ρ_{xy} are very clear at 5 K, showing a positive SMR (FM-like) response, but the temperature dependence is markedly different: $\Delta\rho_{xy}$ diminishes in amplitude upon increasing temperature [**Fig. 2(c)**]. We note here that a thorough analysis of the obtained ADMR were done both for the T' and R' BFO devices, to exclude other commonly known effects such as i) the anisotropic magnetoresistance (AMR) induced by magnetic proximity effects (MPE), ii) weak antilocalization and iii) the Hanle magnetoresistance to the observed SMR. Supplementary Note 2 shows the extended set of measurements and their detailed analysis [39]. Briefly, the AMR effect in Pt due to the MPE is excluded in our measurements by performing experiments with the magnetic field rotating in the out of plane direction (γ) where, due to its geometry, such effects are commonly observed. No appreciable ADMR are observed under γ rotation for both the T' and R' BFO, ruling out the presence of AMR due to MPE effects.

The key finding of *positive* SMR, along with the opposite dependence of the SMR amplitude with temperature, is intriguing and indicative of the different origin of magnetic ordering at the surface of T' BFO and R' BFO. The observed positive SMR in both cases, even though they are nominally (spin canted) AFMs, could arise from various sources. It is unlikely that the magnetic field is purely manipulating $\bf L$, since in this case the sinusoidal modulation of ρ_{xy} would give *negative* SMR. Conversely, whilst the applied $\bf H$ field may provide negligible effect on $\bf L$, it can still increase the canting angle of the wFM, yielding a positive SMR.

We explain the temperature dependence of SMR for T' BFO by incorporating our DFT findings as follows. Since the external magnetic field is applied in plane, SMR is sensitive only to the in-plane magnetization component [18]. According to **Fig. 1(e)**, at low temperature, T' BFO intrinsically has a

vanishingly small value of M_x and M_y ; we thus observe no SMR signal. Upon increasing temperature to 200 K, the applied field induces a non-zero moment, giving a detectable SMR response. Upon further increase of temperature towards the transition at 350 K, the magnitude of the moment induced by the applied field increases, amplifying $\Delta \rho_{xy}$. Essentially, the magnetic susceptibility of T' BFO increases with temperature, giving a larger induced \mathbf{M} under applied field, consistent with the monotonic increase in the SMR from 200 to 370 K.

Next, we describe the temperature dependence of the SMR signal for R' BFO, which is categorized into two regimes: T > 80 K and T < 80 K. The SMR amplitude shows a monotonic decrease with increasing temperature, but, interestingly, below 80 K, it sharply increases. Ignoring for now this sharp upturn, the SMR appears to be consistent with the general downwards trend of the total wFM of BFO [43,44] upon increasing temperature.

We rationalize this behavior as follows. In BFO, ${f M}$ is related to ${f L}$ and the octahedral tilting pseudovector ${m \omega}$ through

$$M \propto L \times \omega$$
. (1)

Here, ω characterizes the octahedral tilting of the unit cell, with the direction giving the axis about which the octahedra rotate in antiphase, and its magnitude giving the rotation in radians [33]. In R-BFO under moderate strain, $\omega \sim //$ [111]. Now, assume that an applied **H** field causes **L** to orient orthogonal to the applied field (see Ref. [31]). For example (neglecting the magnitude of these vectors), if **H** // [100], then **L** // [010], and if ω // [111] [**Fig. 1(e)**], then, according to Eq. (1), **M** // [10 $\overline{1}$]. Here, the in-plane component of **M** is *parallel with the applied field* **H**. If the rotating applied magnetic field causes **L** to rotate synchronously orthogonal to **H**, then the induced **M** (according to Eq. 1) will also oscillate (albeit with some slight angle-dependent amplitude due to varying proportions of in-plane and out-of-plane **M** components).

The key observation is that if **M** is indeed dictated by Eq. 1 (that is, mediated by **L**), then its inplane component will always be aligned with the applied **H** field – giving rise to a seemingly ferromagnetic SMR response. Now, if the total magnetic moment of BFO shows a decrease of magnitude upon increasing temperature [43], then one should anticipate the same decreasing trend in SMR of R' BFO, as observed in **Fig. 2(d)**. Note that for T' BFO, this line of reasoning does not hold, as the octahedral rotation patterns are different [i.e., ω // [110] from **Fig. 1(f)**], and the total magnitude of **M** for T' BFO is much smaller [**Fig. 1(e)**]. For T' BFO upon increasing temperature, the moment induced directly by the applied field (rather than mediated by **L**) dominates the SMR response.

Briefly summarizing the SMR results, we observe SMR for T' BFO that is sizeable at 300 K but negligible at lower temperatures. In contrast, the SMR for R' BFO is strongest at 5 K and monotonically decreases upon increasing temperature. In the latter case, there appears to be two temperature regimes, with a possible transition at around 80 K. To delve deeper and search for possible origins for the two regimes for R' BFO, we performed SMR at different field strengths.

Figure 3 presents field dependent measurements at 300 K for T' BFO, and at 5 K for R' BFO [Fig. 3(a,c)]. Field-dependent data were also taken for R' BFO at 150 K (not shown). For both samples, the extracted $\Delta\rho_{xy}$ shows a linear dependence with field – specifically T' BFO at 300 K [Fig. 3(b)] and R' BFO at 5 K and 150 K [Fig. 3(d)]. According to SMR theory [18], at a given temperature, the SMR signal increases linearly with the induced magnetic moment. The observed linear field dependence of SMR for both T' and R' BFO has three implications. First, it cannot result from domain reorientation, which would give a quadratic field dependence [19]; second, no spin flop transition occurs, as this would yield an abrupt change in the sign of SMR when L reorients with the field; and third, no transition from cycloidal-pseudocollinear AFM takes place, as this would also presumably be manifest in the slope of $\Delta\rho_{xy}$ vs. H. In other words, an applied magnetic field as small as 1 T can manipulate the L vector (to remain orthogonal to the field), but upon increasing field, the only change is the magnitude of the induced magnetic moment.

To conclude, although bulk BFO is a canted cycloidal antiferromagnet (Refs. [3,12]), the observed positive SMR in both cases implies that the experiment probes the weak FM at the surface. The drastically different octahedral rotation patterns for R' and T' results in their **M** vectors to couple to the applied field, each in a unique manner. Consequently, R' BFO and T' BFO show different temperature dependencies, with the SMR enhanced at room temperature for T' BFO. In R' BFO, the weak FM follows the applied field, mediated through the **L** vector. In contrast, and crucially, for T' BFO, the vanishingly small in-plane FM is not locked to **L**, so the moment induced by the applied magnetic field dominates the SMR response thus increasing monotonically with temperature. Nevertheless, the increased SMR at low temperatures for R' BFO warrants further study. It may be that the structural STO phase transition at 105 K modifies the octahedral rotation pattern and/or magnetic order of BFO, a spin-glass transition with blocking temperature ~50 K occurs [45], or below 80 K, BFO develops cycloidal order [46] with its weak FM averaged to zero making it more sensitive to applied field. Further SMR experiments using R' BFO on a substrate without a low temperature

structural transition (like $NdGaO_3$, Ref. [47]), or low temperature NV-center scanning magnetometry [10] could provide insight on this issue.

Author Contributions

T.B., D.S., and V.N. conceived and supervised the study. O.P. fabricated the films and carried out structural characterization. S.C. patterned Hall bars and carried out SMR measurements and analysis with input from J.J.L.vR and T.B. C.X., B.X., and S.X. performed calculations under the supervision of L.B. F.A. and J.J. performed Mössbauer spectroscopy measurements and analysis. D.S and V.N. wrote the manuscript with input from S.C., T.B., B.X. and L.B. All authors discussed the data and contributed to analysis and feedback.

Acknowledgements

This research was partially supported by the Australian Research Council (ARC) Centre of Excellence in Future Low-Energy Electronics Technologies (project no. CE170100039) and funded by the Australian Government. This work is realized using the facilities available at NanoLab NL. S.C. acknowledges funding support from the European Union Horizon 2020 research and the innovation program under grant agreement no. 696656. J.J.L.vR. acknowledges financial support from a Dieptestrategie grant (2019), Zernike Institute for Advanced Materials. S.X. and B.X. acknowledge financial support from National Natural Science Foundation of China under Grant No. 12074277. LB acknowledges support from the Vannevar Bush Faculty Fellowship (VBFF) from the Department of Defense and Award No. DMR-1906383 from the National Science Foundation Q-AMASE-i Program (MonArk NSF Quantum Foundry). F.A. and J.J. acknowledge the support of the Région Normandie and European Regional Development Fund of Normandy (ERDF) through the MAGMA project. We are grateful to M.M. Seyfouri and T. Musso for assistance with figures, and we thank G. Bassett-Smith for critical reading, and M. Bibes for discussions.

References

- [1] J. T. Heron, M. Trassin, K. Ashraf, M. Gajek, Q. He, S. Y. Yang, D. E. Nikonov, Y.-H. Chu, S. Salahuddin, and R. Ramesh, *Electric-Field-Induced Magnetization Reversal in a Ferromagnet-Multiferroic Heterostructure*, Phys Rev Lett **107**, 217202 (2011).
- [2] S. O. Sayedaghaee, B. Xu, S. Prosandeev, C. Paillard, and L. Bellaiche, *Novel Dynamical Magnetoelectric Effects in Multiferroic BiFeO*₃, Phys Rev Lett **122**, 097601 (2019).
- [3] A. Haykal et al., Antiferromagnetic Textures in BiFeO₃ Controlled by Strain and Electric Field, Nat Commun 11, 1704 (2020).
- [4] H. Jang et al., Strain-Induced Polarization Rotation in Epitaxial (001) BiFeO₃ Thin Films, Phys Rev Lett **101**, 107602 (2008).
- [5] I. C. Infante et al., *Bridging Multiferroic Phase Transitions by Epitaxial Strain in BiFeO*₃, Phys Rev Lett **105**, 057601 (2010).
- [6] H. Béa et al., Evidence for Room-Temperature Multiferroicity in a Compound with a Giant Axial Ratio, Phys Rev Lett **102**, 217603 (2009).
- [7] I. C. Infante et al., Multiferroic Phase Transition near Room Temperature in BiFeO₃ Films, Phys Rev Lett **107**, 237601 (2011).
- [8] H. Béa, M. Bibes, F. Ott, B. Dupé, X.-H. Zhu, S. Petit, S. Fusil, C. Deranlot, K. Bouzehouane, and A. Barthélémy, *Mechanisms of Exchange Bias with Multiferroic BiFeO₃ Epitaxial Thin Films*, Phys Rev Lett **100**, 017204 (2008).
- [9] D. Lebeugle, D. Colson, A. Forget, M. Viret, A. M. Bataille, and A. Gukasov, *Electric-Field-Induced Spin Flop in BiFeO*₃ *Single Crystals at Room Temperature*, Phys Rev Lett **100**, 227602 (2008).
- [10] A. Finco et al., *Imaging Topological Defects in a Noncollinear Antiferromagnet*, Phys Rev Lett **128**, 187201 (2022).
- [11] M. Hambe, A. Petraru, N. A. Pertsev, P. Munroe, V. Nagarajan, and H. Kohlstedt, *Crossing an Interface: Ferroelectric Control of Tunnel Currents in Magnetic Complex Oxide Heterostructures*, Adv Funct Mater **20**, 2436 (2010).
- [12] S. R. Burns, O. Paull, J. Juraszek, V. Nagarajan, and D. Sando, *The Experimentalist's Guide to the Cycloid, or Noncollinear Antiferromagnetism in Epitaxial BiFeO*₃, Advanced Materials **32**, 2003711 (2020).
- [13] M. Cazayous, Y. Gallais, A. Sacuto, R. de Sousa, D. Lebeugle, and D. Colson, *Possible Observation of Cycloidal Electromagnons in BiFeO*₃, Phys Rev Lett **101**, 037601 (2008).
- [14] D. Sando et al., Crafting the Magnonic and Spintronic Response of BiFeO₃ Films by Epitaxial Strain, Nat Mater **12**, 641 (2013).
- [15] J. Li et al., Spin Current from Sub-Terahertz-Generated Antiferromagnetic Magnons, Nature **578**, 70 (2020).
- [16] E. Parsonnet et al., Nonvolatile Electric Field Control of Thermal Magnons in the Absence of an Applied Magnetic Field, Phys Rev Lett **129**, 087601 (2022).
- [17] S. Manipatruni, D. E. Nikonov, C. C. Lin, T. A. Gosavi, H. Liu, B. Prasad, Y. L. Huang, E. Bonturim, R. Ramesh, and I. A. Young, *Scalable Energy-Efficient Magnetoelectric Spin—Orbit Logic*, Nature **565**, 35 (2019).
- [18] Y. T. Chen, S. Takahashi, H. Nakayama, M. Althammer, S. T. B. Goennenwein, E. Saitoh, and G. E. W. Bauer, *Theory of Spin Hall Magnetoresistance*, Phys Rev B **87**, 144411 (2013).
- [19] J. Fischer et al., Spin Hall Magnetoresistance in Antiferromagnet/Heavy-Metal Heterostructures, Phys Rev B **97**, 014417 (2018).

- [20] A. Das, V. E. Phanindra, A. J. Watson, and T. Banerjee, *Coexistence of Different Magnetic Ordering in Thin Films of SrMnO₃ Studied by Spin Transport*, Applied Physics Letters **118**, 052407 (2021).
- [21] J. J. L. Van Rijn, D. Wang, B. Sanyal, and T. Banerjee, *Strain-Driven Antiferromagnetic Exchange Interaction in SrMnO₃ Probed by Phase-Shifted Spin Hall Magnetoresistance*, Phys Rev B **106**, 214415 (2022).
- [22] M. Althammer et al., Quantitative Study of the Spin Hall Magnetoresistance in Ferromagnetic Insulator/Normal Metal Hybrids, Phys Rev B **87**, 224401 (2013).
- [23] G. R. Hoogeboom, A. Aqeel, T. Kuschel, T. T. M. Palstra, and B. J. Van Wees, *Negative Spin Hall Magnetoresistance of Pt on the Bulk Easy-Plane Antiferromagnet NiO*, Appl Phys Lett **111**, 052409 (2017).
- [24] L. Baldrati et al., Full Angular Dependence of the Spin Hall and Ordinary Magnetoresistance in Epitaxial Antiferromagnetic NiO(001)/Pt Thin Films, Phys Rev B **98**, (2018).
- [25] S. R. Burns et al., Expansion of the Spin Cycloid in Multiferroic BiFeO₃ Thin Films, NPJ Quantum Mater 4, 18 (2019).
- [26] H. Béa, M. Bibes, S. Petit, J. Kreisel, and A. Barthélémy, Structural Distortion and Magnetism of BiFeO₃ Epitaxial Thin Films: A Raman Spectroscopy and Neutron Diffraction Study, Philos Mag Lett **87**, 165 (2007).
- [27] W. Saenrang et al., Deterministic and Robust Room-Temperature Exchange Coupling in Monodomain Multiferroic BiFeO₃ Heterostructures, Nat Commun **8**, 1583 (2017).
- [28] X. Ke, P. P. Zhang, S. H. Baek, J. Zarestky, W. Tian, and C. B. Eom, *Magnetic Structure of Epitaxial Multiferroic BiFeO₃ Films with Engineered Ferroelectric Domains*, Phys Rev B **82**, 134448 (2010).
- [29] D. Sando et al., Influence of Flexoelectricity on the Spin Cycloid in (110)-Oriented BiFeO₃ Films, Phys Rev Mater **3**, 104404 (2019).
- [30] D. Sando et al., A Magnetic Phase Diagram for Nanoscale Epitaxial BiFeO3 Films, Appl Phys Rev 6, 041404 (2019).
- [31] A. Agbelele et al., Strain and Magnetic Field Induced Spin-Structure Transitions in Multiferroic BiFeO₃, Advanced Materials **29**, 1602327 (2017).
- [32] J. Buhot et al., *Driving Spin Excitations by Hydrostatic Pressure in BiFeO*₃, Phys Rev Lett **115**, 267204 (2015).
- [33] L. Bellaiche, Z. Gui, and I. a Kornev, *A Simple Law Governing Coupled Magnetic Orders in Perovskites*, Journal of Physics: Condensed Matter **24**, 312201 (2012).
- [34] H. J. Zhao, P. Chen, S. Prosandeev, C. Paillard, K. Patel, J. Íñiguez, and L. Bellaiche, *Energetic Couplings in Ferroics*, Adv Electron Mater **8**, 2100639 (2022).
- [35] D. Sando, T. Young, R. Bulanadi, X. Cheng, Y. Zhou, M. Weyland, P. Munroe, and V. Nagarajan, *Designer Defect Stabilization of the Super Tetragonal Phase in >70-Nm-Thick BiFeO₃ Films on LaAlO₃ Substrates, Jpn J Appl Phys 57, 0902B2 (2018).*
- [36] D. Sando, C. Carrétéro, M. N. Grisolia, A. Barthélémy, V. Nagarajan, and M. Bibes, *Revisiting the Optical Band Gap in Epitaxial BiFeO*₃ *Thin Films*, Adv Opt Mater **6**, 1700836 (2018).
- [37] D. Sando et al., Interfacial Strain Gradients Control Nanoscale Domain Morphology in Epitaxial BiFeO₃ Multiferroic Films, Adv Funct Mater **30**, 2000343 (2020).
- [38] A. Agbelele, D. Sando, I. C. Infante, C. Carrétéro, S. Jouen, J. M. Le Breton, A. Barthélémy, B. Dkhil, M. Bibes, and J. Juraszek, *Insight into Magnetic, Ferroelectric and Elastic Properties of Strained BiFeO*₃ *Thin Films through Mössbauer Spectroscopy*, Appl Phys Lett **109**, 042902 (2016).

- [39] See Supplemental Material at [URL Will Be Inserted by Publisher] for Raw Data of Transverse Resistance, Longitudinal Angle-Dependent Magnetoresistance Data, and Fitting of Spin Hall Magnetoresistance Data.
- [40] H. Nakayama et al., Spin Hall Magnetoresistance Induced by a Nonequilibrium Proximity Effect, Phys Rev Lett **110**, 206601 (2013).
- [41] S. Vélez, V. N. Golovach, A. Bedoya-Pinto, M. Isasa, E. Sagasta, M. Abadia, C. Rogero, L. E. Hueso, F. S. Bergeret, and F. Casanova, *Hanle Magnetoresistance in Thin Metal Films with Strong Spin-Orbit Coupling*, Phys Rev Lett **116**, 016603 (2016).
- [42] Y. Niimi, D. Wei, H. Idzuchi, T. Wakamura, T. Kato, and Y. Otani, *Experimental Verification of Comparability between Spin-Orbit and Spin-Diffusion Lengths*, Phys Rev Lett **110**, 016805 (2013).
- [43] V. V. Lazenka, M. Lorenz, H. Modarresi, K. Brachwitz, P. Schwinkendorf, T. Böntgen, J. Vanacken, M. Ziese, M. Grundmann, and V. V. Moshchalkov, *Effect of Rare-Earth Ion Doping on the Multiferroic Properties of BiFeO₃ Thin Films Grown Epitaxially on SrTiO₃ (100), J Phys D Appl Phys 46, (2013).*
- [44] D. Albrecht, S. Lisenkov, W. Ren, D. Rahmedov, I. A. Kornev, and L. Bellaiche, *Ferromagnetism in Multiferroic BiFeO₃ Films: A First-Principles-Based Study*, Phys Rev B **81**, 140401(R) (2010).
- [45] M. K. Singh, W. Prellier, M. P. Singh, R. S. Katiyar, and J. F. Scott, *Spin-Glass Transition in Single-Crystal BiFeO*₃, Phys Rev B **77**, 144403 (2008).
- [46] H. Hojo, R. Kawabe, K. Shimizu, H. Yamamoto, K. Mibu, K. Samanta, T. Saha-Dasgupta, and M. Azuma, Ferromagnetism at Room Temperature Induced by Spin Structure Change in BiFe _{1-x}Co_xO₃ Thin Films, Advanced Materials **29**, 1603131 (2017).
- [47] V. E. Phanindra, A. Das, J. J. L. van Rijn, S. Chen, B. J. van Wees, and T. Banerjee, *Spin Hall Magnetoresistance in Paramagnetic NdGaO*₃, Appl Phys Lett **123**, 022410 (2023).
- [48] A. Aqeel, N. Vlietstra, J. A. Heuver, G. E. W. Bauer, B. Noheda, B. J. Van Wees, and T. T. M. Palstra, *Spin-Hall Magnetoresistance and Spin Seebeck Effect in Spin-Spiral and Paramagnetic Phases of Multiferroic CoCr₂O₄ Films, Phys Rev B 92, 224410 (2015).*

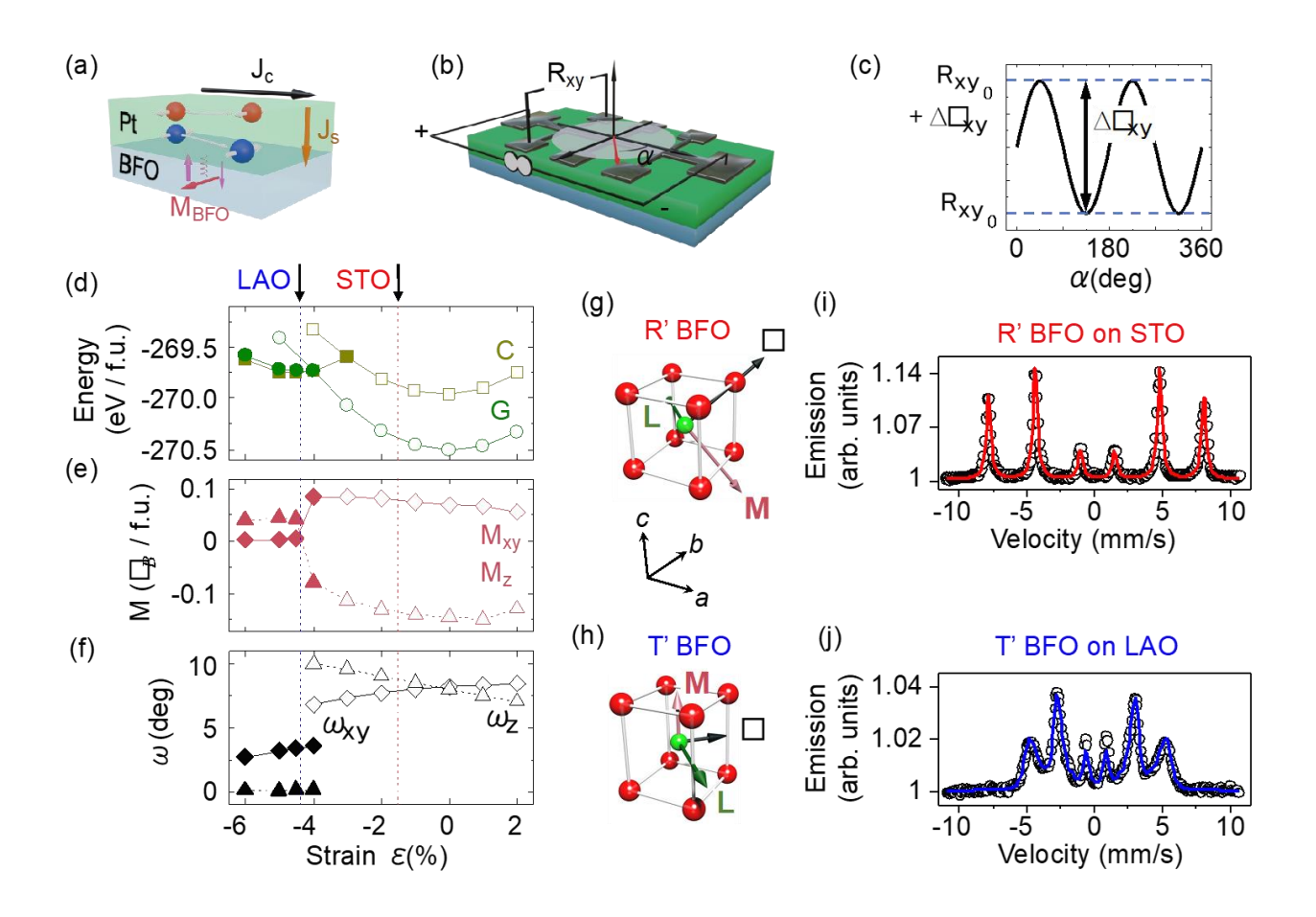


Figure 1. (a) Principle of SMR, (b) measurement of transverse resistivity ρ_{xy} with varying applied magnetic field, (c) dependence of the transverse resistivity on angle α . R_{xy_0} is the minimum value of resistivity. Density functional theory calculated energy (d), magnetization components (e), and octahedral rotations (f) of various magnetic structures in T' and R' BFO phases as a function of strain. (g,h) Schematics of the BFO unit cell (red spheres = bismuth; green spheres = iron; oxygen atoms omitted for clarity) showing direction of vectors ω , L, and M. (i,j) conversion electron Mössbauer spectra (at 300 K) of R' and T' BFO films. f.u. = formula unit.

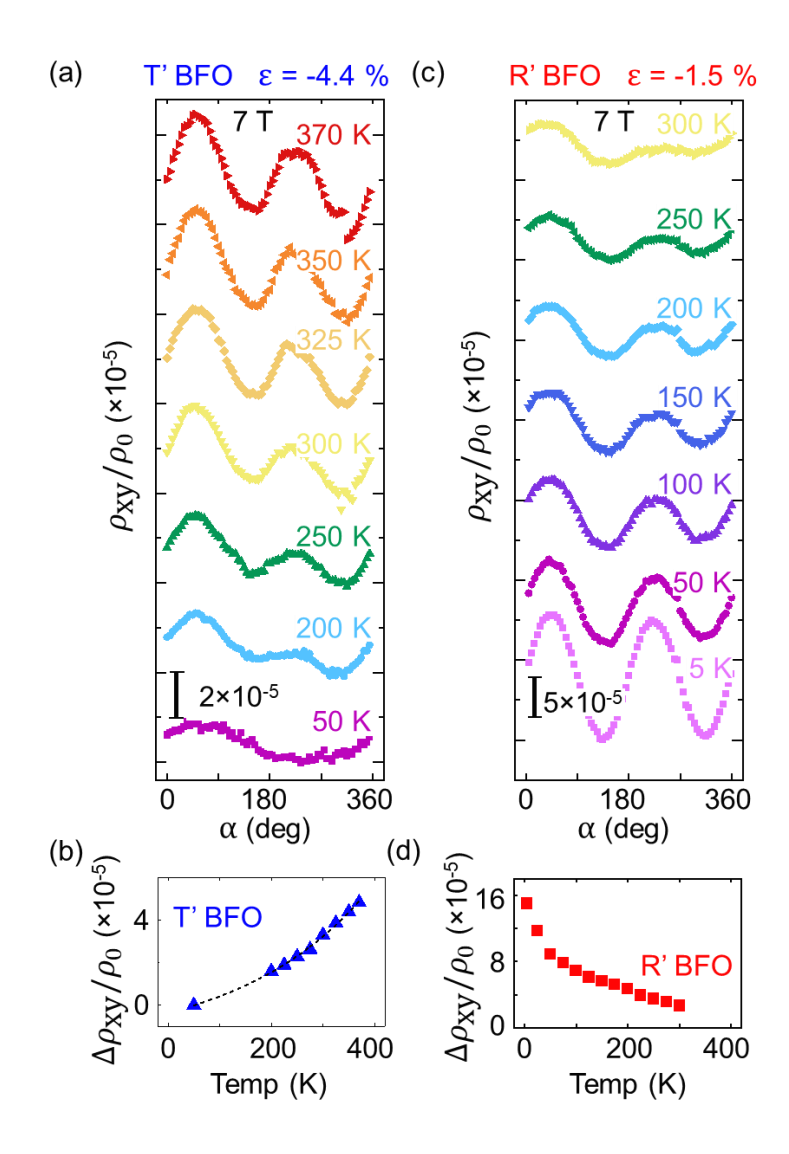


Figure 2. (a) T' BFO SMR response and (b) temperature dependence of normalized $\Delta \rho_{xy}$. (c) R' BFO SMR response and (d) extracted $\Delta \rho_{xy}$. The additional 360° periodicity with the 180° SMR periodicity comes from a small out-of-plane Hall component related to slight misalignment of the in-plane rotator (Ref. [48]). The discontinuity in the data for 370 K in (a) arises from slight thermal drift in our setup.

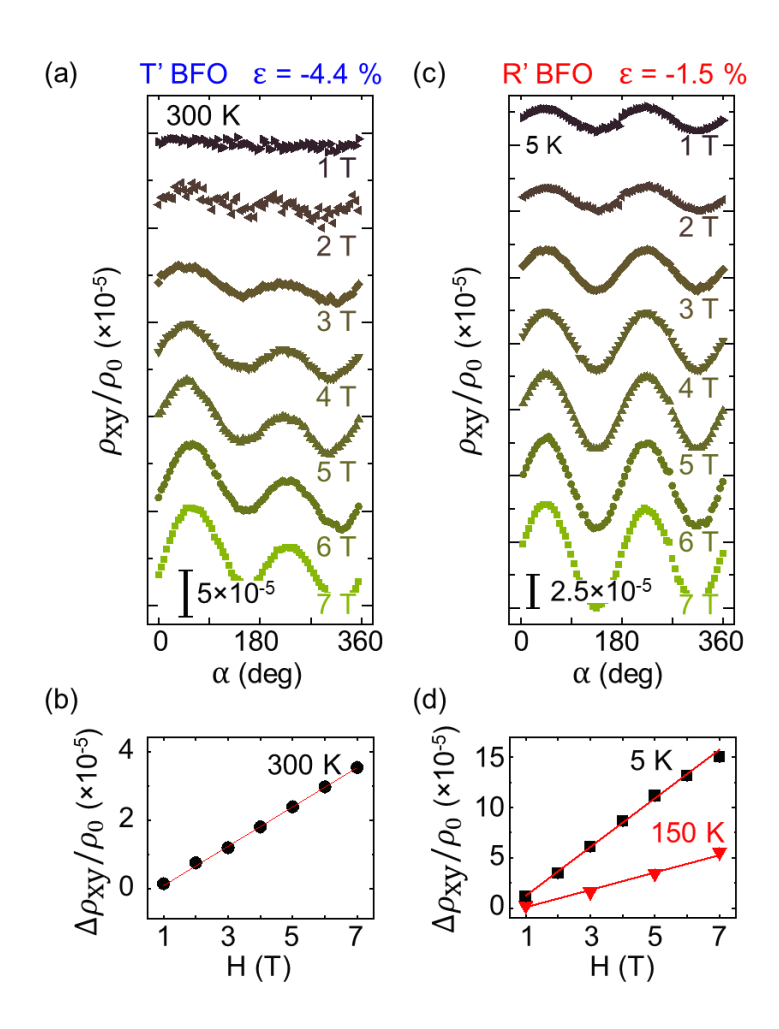


Figure 3. Field dependence of (a) ρ_{xy} and of (b) $\Delta\rho_{xy}$ for T' BFO at 300 K, (c) field dependence of ρ_{xy} at 5 K and (d) $\Delta\rho_{xy}$ at 5 K and 150 K for R' BFO.